Advanced Steel Construction – Vol. 17 No. 3 (2021) 273–282
DOI:10.18057/IJASC.2021.17.3.6

CAPACITY EVALUATION OF EIGHT BOLT EXTENDED ENDPLATE MOMENT CONNECTIONS SUBJECTED TO COLUMN REMOVAL SCENARIO

Ehsan Ahmadi [1, 2] and Seied Ahmad Hosseini [3, *]

[1] *Department of Civil Engineering, Islamic Azad University, Tehran, Iran*
[2] *Beton Wall Co., Tehran, Iran*
[3] *Faculty of Passive Defense, Malek Ashtar University of Technology, Iran*
** (Corresponding author: E-mail: hoseini@mut.ac.ir)*

ABSTRACT

The extended stiffened endplate (8ES) connection is broadly used in the seismic load-resisting parts of steel structures. This connection is prequalified based on the AISC 358 standard, especially for seismic regions. To study this connection's behaviors, in the event of accidental loss of a column, the finite element model results were verified against the available experimental data. A parametric study using the finite element method was then carried out to investigate these numerical models' maximum capacity and effective parameters' effect on their maximum capacity in a column loss scenario. This parametric analysis demonstrated that these connections fail at the large displacement due to the catenary action mode at the rib stiffener's vicinity. The carrying capacity, PEEQ, Von-Mises stress, middle column force-displacement, critical bolt axial load, and the beam axial load curves were discussed. Finally, using the Least Square Method (LSM), a formula is presented to determine the displacement at the maximum capacity of these connections. This formula can be used in this study's presented method to determine the maximum load capacity of the 8ES connections in a column loss scenario.

ARTICLE HISTORY

Received: 9 July 2020
Revised: 25 March 2021
Accepted: 30 March 2021

KEYWORDS

Bolted endplate connection;
Finite element analysis;
Catenary action;
Column loss scenario;
Theoretical model

1. Introduction

The need for structural resistance against progressive failure became obvious after the progressive collapse of famous towers globally, and structural safety has become one of the most significant worries in the design of structures. Based on the definition of progressive collapse in the GSA design code [1], progressive collapse is the local damage of a structural element that causes connected components' failure. Therefore, the overall failure of the structure is much greater than the initial damage. In the last few decades, researchers realized that by providing sufficient continuity, ductility, and indeterminacy in the structures, they could prevent this phenomenon. Besides, different standards development committees were attracting to revising the standards' design procedure that only local failure was happening in the structure. The GSA [1] and the US Department of Defense (DOD), and the UFC [2] conducted comprehensive research in this field.

One of the effective solutions mentioned in these guidelines to decreasing the damage caused by progressive collapse is the alternate load path method (APM). In this method, after abnormal load damage a middle column, the structure seeks an alternative load path to survive from major collapse by redistributing this load on damaged members with a catenary action mechanism. Fig. 1 shows the formation of catenary behavior in the beams due to the column's sudden removal. At the first stage, the beams resist the vertical loads through their flexural stiffness, and then as the displacements increase downwards, the beams act as cables between the columns, creating significant tensile forces that the beam-column joints must be able to resist [3]. It should be noted that the demand created in a column removal scenario is different from the earthquake situation. In fact, in these two situations, the internal forces generated to affect the structure's behavior. Therefore, evaluating beam to column joints in a column removal scenario is essential to preventing progressive collapse [4]. Although extensive research studies have been done according to the behavior of connections under different loading type and boundary conditions, up to now, many of these research are related to welded joints or connections under seismic loads, and very few ones are about beam to column bolted steel joints under column removal scenario. In the following paragraphs, some of these research are reviewed.

AstanehAsl et al. [5] have conducted four full-scale tests to investigate the cable-supported floor's catenary action in a column removal scenario. The test indicates that using the cable on the floor could extend the middle column's catenary action and displacement. Khandelwal and El-Tawil [6] carried out the numerical investigation on the welded connections to evaluate the parameters which affect the formation of catenary action. Their study shows that in the special steel moment frame, which is designed seismically, parameters like the beam depth or detail of the beam's web to column play a significant role in a column removal scenario. Also, Sadek et al. [7] conducted a comprehensive study of steel moment connections subjected to column removal scenario to investigate welded connections similar to Khandelwal and El-Tawil [6]. In 2008, Demonceau [8] carried out an experimental test to investigate two main objects: the progress of catenary action and the study of the behavior of connections subjected to conventional loading. The performance of welded moment connection and side-plate moment connections subjected to blast load was investigated by Karns et al. [9] in experimental test and numerical modeling analysis. Yang and Tan [10-13] investigated experimental and numerical simulations to evaluate the behavior of various simple and semi-rigid connections. They indicated that as the current acceptance criteria consider connections test for flexural only, the rotation capacity for these connections is too conservative, and component-based models are essential to designing structures in a column removal scenario. In 2018, Meng et al. [14] conducted an experimental and numerical analysis on welded unreinforced flange-bolted web connections to investigate these connections' performance with two beams and three columns with different span ratios against column removal scenario. According to the progressive collapse and column removal scenario, further studies can be found in [15-20].

Also, some experimental tests were done by Yan et al. at the University of Sydney to investigate the behavior of steel connections such as bolted endplate and double web angle connections. The tests were conducted until the failure of connections to investigate their behavior's full range [21]. Faridmehr et al. [22] done some experimental tests for examining the classification index of endplate connections. They suggested a new classification index for these connections based on the rigidity, ductility requirement, and capacity level. More experimental and numerical investigation was done by Jayachandran et al. [23] to evaluate the behavior of bolted endplate connections. Their study had eight endplate connections with extended endplate in tension side, which then simulated using ABAQUS software and validated by experimental data to reconsider the Frye-Morris polynomial model.

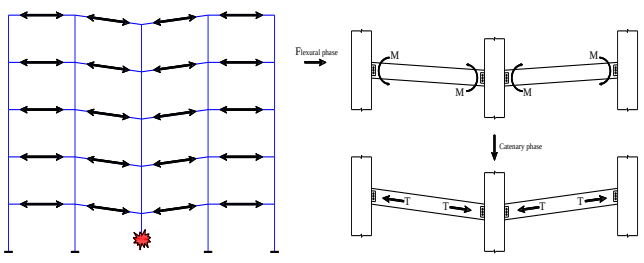

Fig. 1 Schematic formation of catenary action in beams [3]

Regarding the presented previous paragraphs, an insignificant number of researchers investigated the behavior of bolted steel moment connections against the column removal scenario, and most research has been done on welded joints. Moreover, the literature review recommends that one of the key mechanisms is considering catenary action in the column removal analysis, which leads to extending a system's capacity in progressive collapse. Therefore, the finite element models of an endplate connection with two beams and three columns were established using ABAQUS software to verify the numerical model. Material constitutive models, element types, material and geometric nonlinearity, and contact models for bolts and endplates were well proposed. Based on the numerical verification, nine 8ES connections subjected to catenary action under a middle column-removal scenario were created using ABAQUS software. These connections are made by welding the beam to an endplate section with the endplate's attachment to a column flange using fully tensioned bolts. Finally, the behavior of these nine numerical models, Von-Mises stresses, plastic equivalent strain (PEEQ), vertical load-displacement curves, the fracture modes, and their maximum capacity under removal of the middle column was evaluated, and at the end, a proposed formula to calculate the maximum capacity of these connections under column removal scenario has been conducted.

2. Finite element verification

The FEM assumptions were verified with the experimental test conducted by Dinu et al. [24]. These experimental tests contain four different connections designed and fabricated to investigate the behavior of steel frame joints subjected to the column removal scenario. They were extracted from a three-bay, four-span plan, and six-story structure with a height of 4000 mm for each story. The beam length was decreased from 8000 mm to 3000 mm as there was space limitation in the laboratory [24]. Also, in all experimental tests, the HEB260 was used for column sections with the reduced flange's width of 160 mm, and the beam section was IPE220. Fig. 2 illustrates the test setup and the lateral braces' locations in the test setup, which resist the specimen's out-of-plane movements in ref [24].

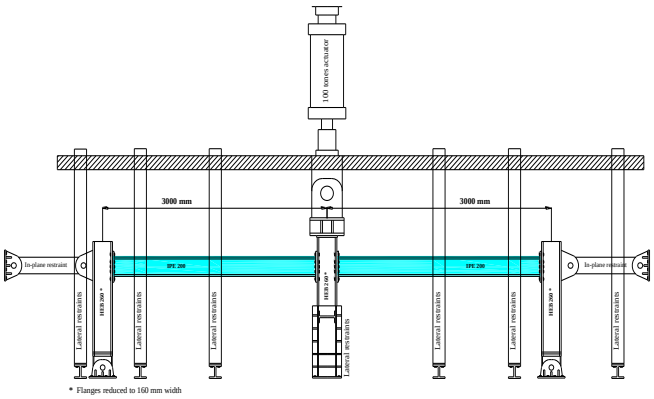

Fig. 2 The test setup used in ref [24]

2.1. Generality

The specimen EP of Ref. [24] was model by ABAQUS software [25] to verify the adopted assumptions for FE modeling. For this specimen, the geometrical properties are shown in Table 1. It was an interior connection that a 100 tons actuator on top of the middle column used to test the specimen under monotonic loading. Fig. 3 presents the geometrical details of specimen EP in mm dimensions and its photo before loading.

Table 1
Geometrical properties of specimen EP in ref [24]

Specimen	EP	**Beam section**	IPE 220
Connection type	Interior	**Column section**	HEB 260*
End-plate	Dimensions (mm)		370 × 130 × 16
Bolts	No.		10
	Diameter (mm)		16

*The width of the flanges reduced to 160 mm.

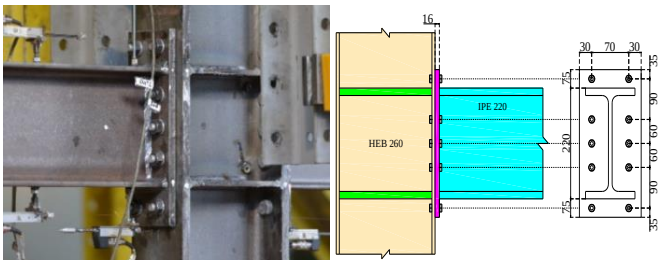

Fig. 3 Photos of specimen EP before the test and geometrical details used by [21]

(dimensions are in mm)

Fig. 4 shows the finite element model of specimen EP, which contains four main parts: columns, beams, endplates, and bolts. The bolts are modeled as a single part made of three partitioned zones: the shank, the head, and the nut. The welds are considered rigid and modeled by a tie contact tool, and they are used to connect the beam to the endplate.

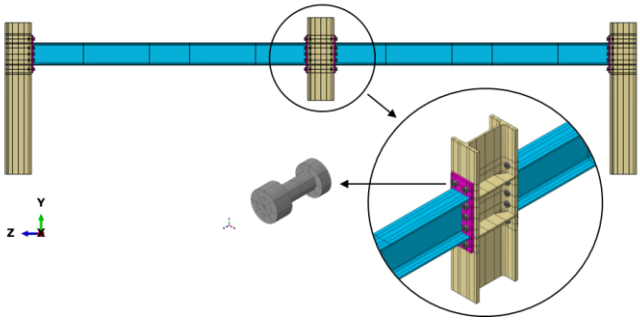

Fig. 4 Finite element model of specimen EP

Due to complex numerical problems in finite element modeling, contacts between system components usually need special care, so small surface-to-surface sliding was used in all system component interactions. In this sliding process, only in the initial stage, the contact defined between the master and slave nodes [26]. It should be noted that the contacts were defined between different part of the system like the column flange and endplate, the bolt nuts and heads with column flange and endplate, and the hole and bolt shanks of both column flange and end plate by surface to surface formulation to simulate component's interaction. In normal behavior, the "hard" contact law with allowed separation after contact was defined. Besides, tangential behavior contacts with "Penalty" law with a slip coefficient of 0.3 is assumed.

The general static procedure was used in finite element modeling using the ABAQUS standard solver. In the "Initial" step, boundary conditions are defined. In the "Pretension" step, the force in a tightened bolt is modeled using the bolt load tool. Two methods can apply this load: Applying specification force or a change in the shank length of bolts. In this study, using the apply force method and the minimum pre-tensioning load presented in table J3.1 of AISC 360-16 [27], the tension in a tightened bolt is modeled. Finally, monotonic loading was applied to the middle column section to simulate the column loss action.

The C3D8R elements with a reduced integration point are used for the verification model. Also, to have a regular shape for elements, especially in critical locations like bolt shanks, holes, and connection locations (200 mm from left and right of connection), the structured meshing technique is used. The mesh sensitivity analysis shows that accurate simulation results can be achieved with the 5 mm mesh size for bolt and hole regions. Also, the mesh size was increased from 10 mm in connection regions to 50 mm in the regions with low strain. The other important part of specimens was modeled with three, two, and two elements in their thickness. Fig. 5 shows the typical finite element mesh of the test specimen.

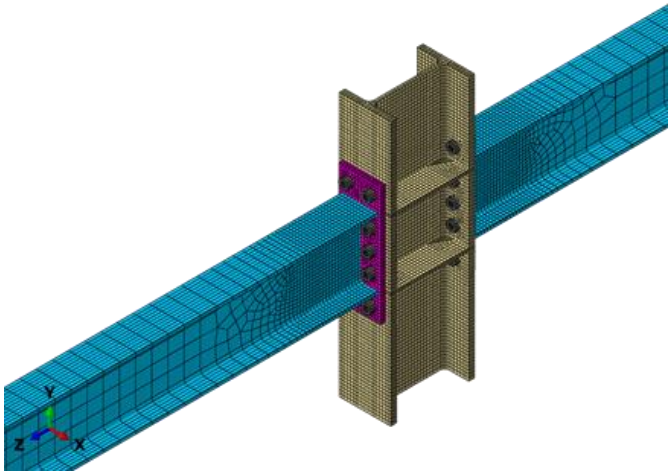

Fig. 5 Typical finite element mesh of the specimen EP

2.2. Materials properties and boundary conditions

The material properties were defined from the basis of given test results in ref [24]. Table 2 presents engineering stress-strain values for specimen EP. These values converted to the true stress-strain relationship using Eq. 1 to Eq. 3 with combined isotropic/kinematic hardening rule. In these equations, ε_{norm} and σ_{norm} are the strain and stress obtained from the coupon test, ε_{true} and σ_{true} are the true strain and stress, and ε_{true}^{pl} is the true plastic mechanical strain.

Table 2
Engineering stress-strain values for different elements of specimen EP used in ref [24]

Component		F_y (Mpa)	F_u (Mpa)	$\varepsilon_{fracture}$ (%)
Beam	Flange	351	498	22.1
	Web	370	497	25.2
Column	Flange	393	589	19.5
	Web	402	583	20.2
Endplate		305	417	30.9
Bolt		965	1080	10.21

$$\varepsilon_{true} = ln\,(1 + \varepsilon_{norm}) \quad (1)$$

$$\sigma_{true} = \sigma_{norm}\,(1 + \varepsilon_{norm}) \quad (2)$$

$$\varepsilon_{true}^{pl} = \varepsilon_{true} - \frac{\sigma_{true}}{E} \quad (3)$$

The boundary conditions are defined similarly to those shown in Fig. 6 to model the appropriate structural behavior under a column removal event. The column tip section at both ends of exterior columns and the top of the interior column are attached to a point and placed into the center of their cross-section. All DOFs of the exterior column are restrained, and the column loss action is simulated by applying static vertical displacement at the interior column reference point until the connection failure.

2.3. Fracture mechanisms

Generally, metals and alloys' failure can be divided into two main categories; ductile and brittle failure. The ductile fracture usually involves a large amount of plastic deformation, warning before fracture, and displays in various ways depending on the material classification, boundary conditions, and constraint level.

On the other hand, brittle failure has small deformation and occurs suddenly in a location. The specimen Ep, which is used in the verification section, may experience various modes of failure (e.g.) the rupture of the weld line at the bottom of the beam flange, net section rupture at the endplate, bolt fracture, or beam flange rupture. Despite different types of fracture mechanisms and methods to simulate the damage in the finite element model, which can be found in the previous work done by Hedayat et al. [28], the focus of this paper is on the two types of methods to capture these damages. Firstly, the extended finite element method (XFEM) [29] use to capture the brittle fracture in the model (fracture of bolts), and secondly, the PEEQ index captures the highest fracture potential locations, especially for ductile fracture.

In the first category, a predefine failure mechanism was used to capture the fracture of bolts. This mechanism consists of two-part: the damage initiation and damage evolution law. Regarding these two parts of the failure mechanism, a nominal quadratic strain (QUADE) for damage initiation and energy-based damage for evolution law was used to verify the specimen [28]. An element's damage initiation can be captured in the second category by observing the stress or strain level at different components. Based on the Hedayat et al. [28] research, the value of PEEQ in the critical parts can be monitored to recognize the fracture's initiate of elements and obtained with the results of coupon tests. The average PEEQ for these components was 0.6 and 0.4 for two steel types of A36 and A572 plates. In this research, the fracture initiates when any location reaches the mentioned PEEQ limits. The plastic equivalent strain index is defined as Eq. 4. This index is used to evaluate nonlinear strain damage and is defined as follows:

$$PEEQ = \frac{\sqrt{\frac{2}{3}\varepsilon_{ij}^{p}\varepsilon_{ij}^{p}}}{\varepsilon_y} \quad (4)$$

Where ε_{ij}^{p} and ε_y are the plastic strain and yield strain, respectively. This method had used to identify the failure of steel components such as shear tab and bolt in simple conventional connections, and in welded connections, beam flange, and web, in other researcher's studies [30-36].

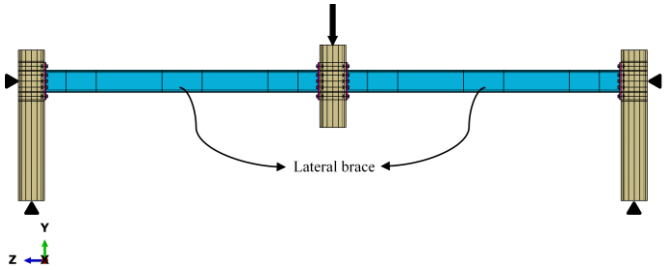

Fig. 6 Boundary conditions applied to finite element models

2.4. Verification results

The finite element model was built using strategies mentioned in previous sections and validated against the experimental results of specimen EP presented in reference [24] regarding the force and displacement relationship. As shown in Fig. 7, the initial stiffness, yield strength, accumulated plastic deformation, and local buckling have good agreement in both experimental and analytical results.

According to experimental results, the bending deformation of the endplate near the central column connection was caused yielding to initiate at vertical displacement and an applied load of 39 mm and 117 kN. After that, flexural stiffness started to decrease dramatically and reach the purely flexural stage (the axial force in the beams was nearly zero) with vertical displacement of 154 mm and applies a load of 175 kN. Finally, the specimen experiences a sudden strength loss by initiating fracture in the bolts in the right beam connection's external bottom row (near the central column). These failure modes are similar to the numerical results, as shown in Fig. 8a and Fig. 8b. As shown in this figure, the proposed fracture mechanism explained in previous sections could provide a quite accurate prediction for bolts' fractures.

Overall, the analytical model shows sound accuracy to predict the experimental results. Also, it is used to investigate the failure mechanism of extended endplate connections.

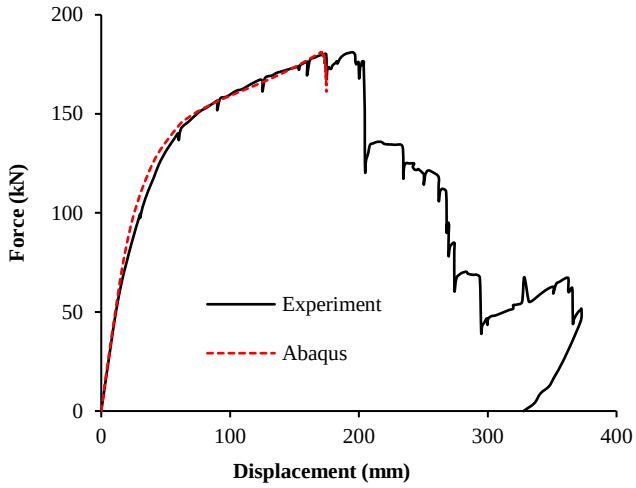

Fig. 7 Comparison between the numerical and experimental results of specimen EP presented in ref [24]

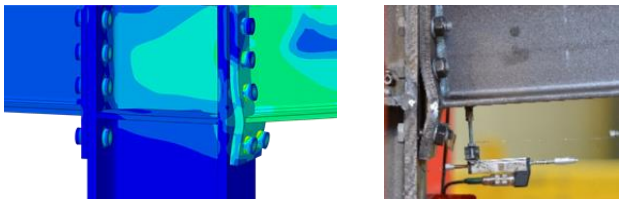

(a)

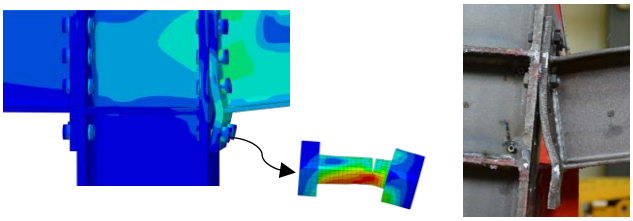

(b)

Fig. 8 Comparison of experimental test and simulation result's failure modes: a) bending deformation of the endplate, b) fracture of the bolt in the middle column connection

3. Connection design and modeling

In the previous sections, the numerical simulation was described for verifying the experimental test done by reference [24]. To investigate the capacity of different 8ES connections in a column removal scenario, a set of nine connections were designed with the lateral load-bearing system of the special moment-resisting frame. For the design of steel elements and the connections AISC 360-16 [27], AISC 341-16 [37], and AISC 358-16 [38] have been used. In the connections design, three different beam sections of W21, W24, and W30 with the column section of W14 were used. The bolts are A490 bolts with diameters of 1, 1 1/8, and 1 1/4 inch, and their threads are excluded from the shear plane. The beams length calculated with the ratio of L_{beam}/d_{beam} = 12 and column length consider as 13 ft for each specimen. A dead and live load of 96 psf and 50 psf proposed for calculating gravity loads, respectively. Table 3 shows the geometry and connection parameters of nine specimens. According to this table, beams depth was varied from 530 to 767 mm, which cause to have a beam length of 6400 to 9083 mm. It should be mentioned that width-to-thickness ratios for beam and column elements are limited to AISC 341-16 [37] criteria, which are related to highly ductile members.

According to the guidelines presented in the UFC [2], the frames during a column removal scenario can be divided to direct influence and indirect influence regions (see Fig. 9a). In this study, the primary region for capacity evaluation of connections is the direct influence area. To this end, the simplified model with an interior column in the center of the model and two adjacent beams can be considered a double full-span assembly, which can be seen in Fig. 9a. Due to the column's small horizontal deformation and compression, the side columns' boundary conditions are simplified to fixed hinge constraints [16, 39-41]. As there is symmetry in the geometry and loading, for all specimens in this study, the boundary conditions for numerical models were considered as those shown in Fig. 9b.

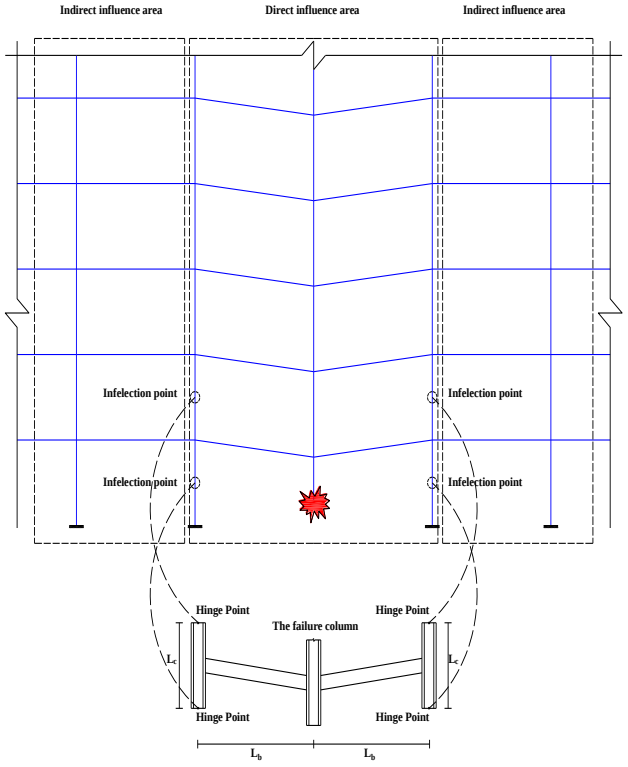

(a)

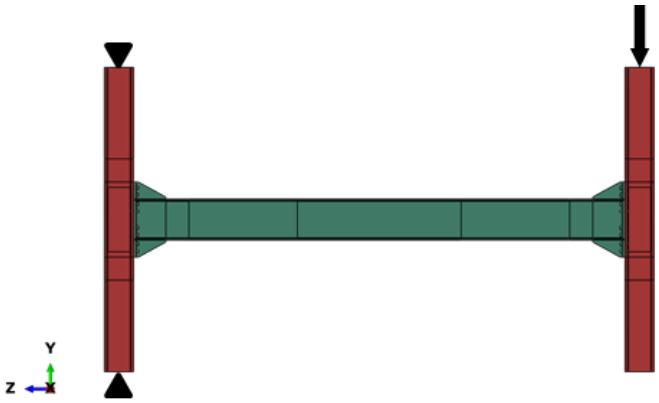

(b)

Fig. 9 a) The double full-span assembly extracted from steel frame b) The typical FE model of numerical specimens

The displacement-controlled loading was considered in the analysis procedure, so a vertical displacement was gradually applied to the removed column until the fracture occurred. It should be noted that this column could only have vertical displacement. Besides, in FE modeling, beams' lateral bracing is provided following the AISC 341-16 [37] to resist the affected beams' out-of-plane movements. In this study, specimens were modeled and analyzed using ABAQUS software ver. 6.14 [25]. The finite element model overview with proposed boundary conditions and the connection components can be seen in Fig. 10.

Table 3
Investigated specimens' details

Model No.	Beam					Column		Endplate			Bolt
	Section	d_{beam} (mm)	b_f / t_f	Z_x (mm^3)	L_{beam} (mm)	Section	d_{column} (mm)	L_p (mm)	b_p (mm)	t_p (mm)	d_{bolt} (mm)
Specimen 1	W21x62	533.4	6.699186992	2359737.216	6400.8	W14x159	381	977.9	254	34.925	25.4
Specimen 2	W21x73	538.48	5.608108108	2818575.008	6461.76	W14x176	386.08	982.98	254	38.1	25.4
Specimen 3	W21x93	548.64	4.52688172	3621541.144	6583.68	W14x233	406.4	993.14	254	34.925	28.575
Specimen 4	W24x76	607.06	6.610294118	3277412.8	7284.72	W14x193	393.7	1051.56	304.8	31.75	25.4
Specimen 5	W24x94	617.22	5.182857143	4162314.256	7406.64	W14x257	416.56	1061.72	304.8	34.925	28.575
Specimen 6	W24x103	622.3	4.591836735	4588377.92	7467.6	W14x283	424.18	1066.8	304.8	34.925	31.75
Specimen 7	W30x108	756.92	6.907894737	5669924.144	9083.04	W14x311	434.34	1201.42	304.8	34.925	31.75
Specimen 8	W30x116	762	6.176470588	6194310.192	9144	W14x342	444.5	1206.5	304.8	38.1	31.75
Specimen 9	W30x124	767.08	5.64516129	6685922.112	9204.96	W14x370	454.66	1211.58	304.8	38.1	31.75

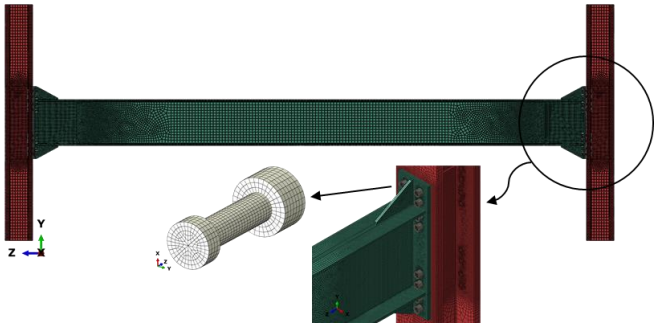

Fig. 10 Typical finite element model of a connection

4. Results and discussion

Nine numerical models for investigating the behavior of 8ES connections were designed and model using ABAQUS software. In this section, these nine models' behavior under the column removal scenario and the effects of effective parameters on connections capacity are discussed. The parameters which directly or indirectly can affect the connection behavior could be d_{beam}, $b_{f\text{-}beam}/t_{f\text{-}beam}$, and $Z_{x\text{-}beam}$. The performance of specimen 1 depicts in Fig. 11. Equivalent plastic strain (PEEQ) contours and Von-Mises stress contours are shown for the overall finite element modeling at the first fracture time step of the analysis for this specimen in Fig. 11a and Fig. 11b, respectively. Based on the research done by [30, 31] and the present study, the high plastic strain and stress demands in the beam flange near the stiffener rib make the 8ES connections susceptible to fracture. According to damage mechanisms, which are supposed in section 2.3, as PEEQ in half of beam flanges width reaches 0.4, fracture initiated and specimen experience the maximum deflection. Understanding the local failure mechanism is highly dependent on the design of these connections, hence based on the design of the connections, it can be seen in Fig. 11a, the plastic hinge in specimens is near the rib stiffener, and plastic deformations are mainly in this region. Due to the plastic hinge formation, local buckling occurred in the beam's flange and web near the stiffener rib. Fig. 17 plotted the deformation, PEEQ, and Von-Mises stress contour for nine specimens.

The Force-displacement curve illustrates specimen 1 at the onset of the first fracture in the bottom beam flange in Fig. 11c. Also, the maximum and fracture point of the specimen has shown in this figure. These points indicate the maximum ductility and strength capacity of this specimen, which later derives the proposed formula. Another important curve to monitoring the critical bolt fracture is Fig. 11d, which illustrates the bolt axial load versus connection displacement at the first fracture's onset. As can be seen in this figure, at the first stage, the bolt pretension load was applied (285000 N) based on the type (A490) and diameter (1 inch) of the bolt. Then, increasing the middle column's deflection, the bolt axial force has increased to the maximum point at the pure flexural stage (no tensile force in beams). After that, due to the plasticization of beam flange elements, the bolt axial force becomes constant. Finally, by the initiation of fracture in the beam flange, the bolt axial load starts to decrease until the full fracture of the beam flange.

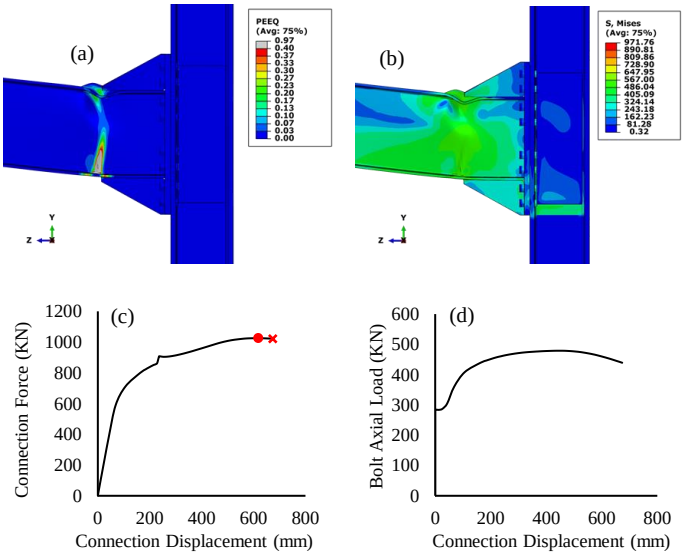

Fig. 11 Performance of the specimen 1 a) Equivalent plastic strain distributions (PEEQ) b) Von-Mises stress c) Force-displacement curve, d) Bolt axial load versus connection displacement at the onset of the first fracture

Comparison of the vertical displacement–force diagrams are shown in Fig. 12 for nine connections with different properties. Based on the connection's properties presented in Table 3, they were divided into three main groups with different beam depths (W21, W24, and W30). It should be noted that the significant effect of the plastic section modulus and the value of the beam flange width to its thickness (b_f/t_f) has caused a capacity increased in specimen 3 compared to specimens 4 and 5.

4.1. The effect of parameter d_{beam}, Z_x, b_f/t_f, and d_{bolt} on the maximum capacity of specimens

As noted earlier, these connections act so that the major capacity depends on the beam properties due to beam flange failure in a column removal scenario. As a result, four parameters of d_{beam}, Z_x, b_f/t_f, and d_{bolt} that mainly affect these connections' capacity have been studied. According to Fig. 13, the value of these four parameters versus each specimen's maximum capacity ($P_{FE\text{-}max}$) is plotted. For instance, Fig. 13a shows that with increasing parameter d_{bean}, the system's overall capacity increases. Also, one of the significant parameters is the beam plastic section modulus (Z_x). As can be seen in Fig. 13b, the maximum values of the system capacity are directly related to the plastic section modulus, and even in specimen 3, the system capacity has increased compared to the specimens with higher beam depth which shows the significant role of this parameter in the capacity of connections in the column removal scenario.

Moreover, increasing the size of bolts diameter, the rigidity of connections, and the overall capacity of connections increased. On the other hand, the ratio of the beam's parameter flange width to its thickness (b_f/t_f) has a vice versa

effect on the maximum capacity of specimens (Fig. 13c). As this ratio increases, the slenderness of flanges increases, and buckling in the beam flange section will happen sooner.

Fig. 14 shows the regression method results and the values of multiple R regarding these connections' capacity. As can be seen in this figure, parameters like the cross-section of the beam (A), beam depth (d_{beam}), flange Width (b_f), plastic section modulus (Z_x), and bolt diameter (d_{bolt}) have a correlation coefficient of more than 80%. It shows, in these connections, the properties of the beam and the diameter of the bolt have a great effect on the connections' capacity.

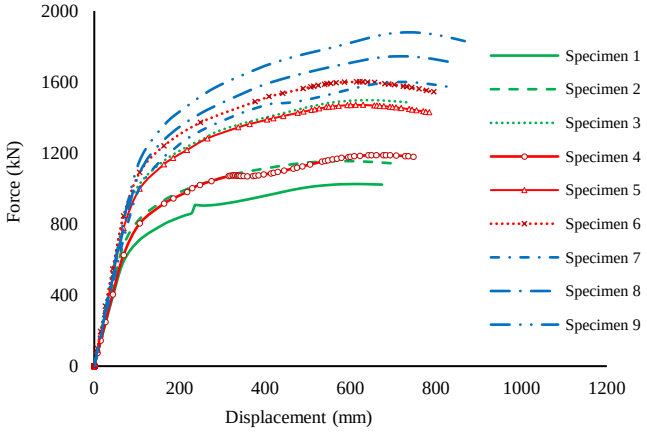

Fig. 12 Connection force-displacement curve of the nine numerical model

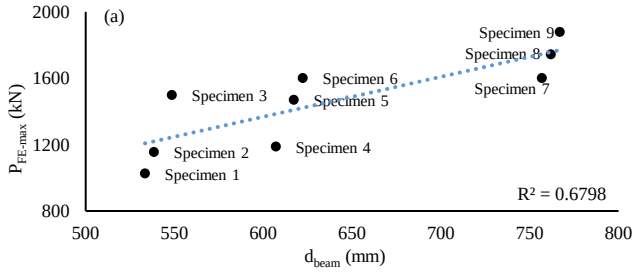

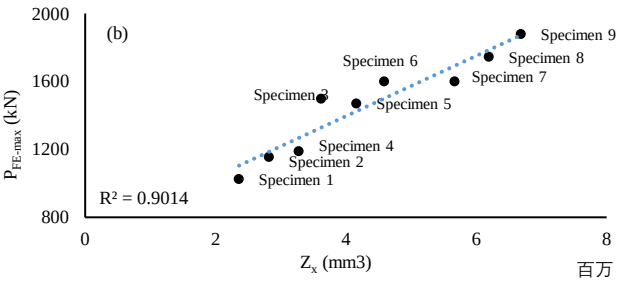

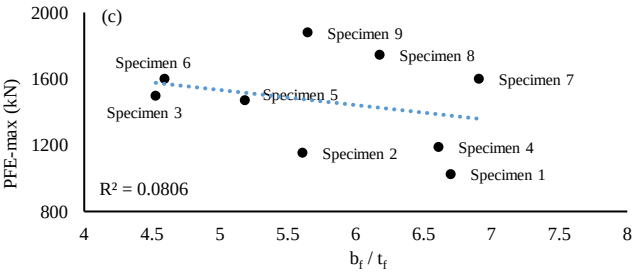

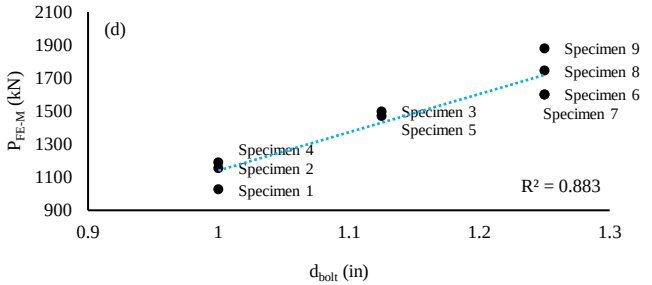

Fig. 13 The effect of parameter a) d_{beam}, b) Z_x, c) b_f/t_f, and d) d_{bolt} on the maximum capacity of specimens

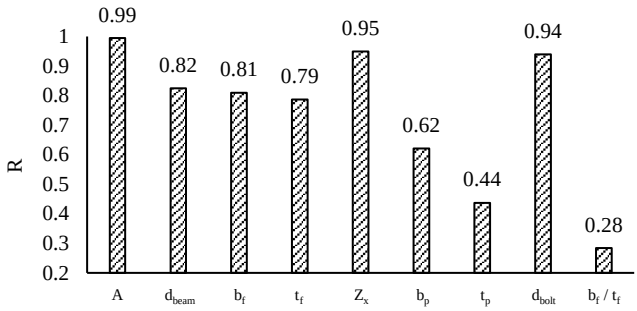

Fig. 14 The values of multiple R regarding the capacity of 8ES endplate connections

Table 4 summarized the connection force and displacement of specimens at the maximum and fracture points. In this table, the second and third columns represent the displacement at the maximum force point and the maximum capacity of different specimens. The two last columns of this table show the displacement and force at the fracture point for specimens.

Table 4
Summary of the force and displacement of all specimens in the maximum and fracture points

Model No.	Δ_{FE-max} (mm)	P_{FE-max} (kN)	Δ_{FE} (mm)	P_{FE} (kN)
Specimen 1	618.72	1025.32	673.71	1022.03
Specimen 2	573.05	1154.41	697.47	1141.81
Specimen 3	636.44	1497.59	734.83	1484.65
Specimen 4	659.83	1188.48	747.14	1179.48
Specimen 5	611.77	1470.46	784.71	1428.38
Specimen 6	614.37	1600.18	794.88	1543.79
Specimen 7	721.70	1599.93	826.77	1573.49
Specimen 8	726.48	1744.25	843.41	1706.50
Specimen 9	739.11	1879.32	867.26	1829.81

4.2. Effect of catenary action on the capacity of specimens

If the connections have adequate ductility, under large deformations due to the column removal scenario, significant axial forces are created in the beams, which is very useful in increasing the system's resistance. This phenomenon is called catenary action. The formation and expansion of catenary action in beams remove the column due to an unusual event. The system is starting to move down due to heavy loads at the location of the removed column. Initially, the beams resist the vertical loads through their flexural stiffness, and as the displacements increase downwards, the upper and lower axis of beams are yielded, and then the range of tensile stresses in the beam axis will increase at the cross-section. At very high displacements, the compressive stresses are eliminated, and the entire cross-section of the beam is in tension. At this point, the beams act as cables between the columns, creating significant tensile forces that the joints must be able to resist.

According to the important role of catenary action in increasing the maximum structure's capacity in a column removal analysis, the system forces versus rotation capacity of specimen 1 is created in three states (see Fig. 15); the

overall force (black line), beam axial force (blue dashed line), and force resulting from flexural stiffness (red dotted line). It should be noted that the P-catenary action obtains through the cut inserted in the cross-section of the beam and Eq.5 and the P-bending calculate by Eq.6 and Eq.7. In these equations the M_{left} and M_{right} are the moments which are obtained from an inserted cut near the stiffener and the L_h is the distance between plastic hinge locations based on the AISC 358-16 [38].

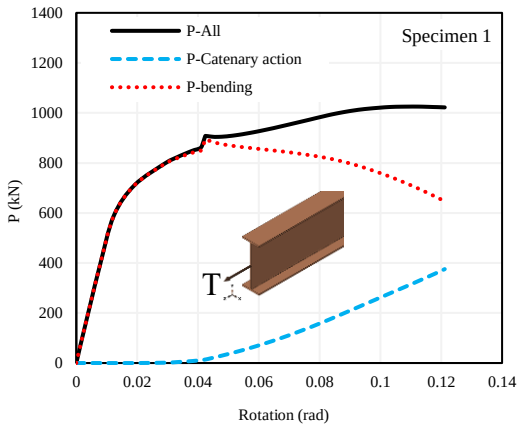

Fig. 15 Force–rotation angle curves of the specimen 1

$$\text{P- Catenary action} = 2 \times T \times \sin(\theta^{*}) \quad (5)$$

*θ → The rotation of connection (Fig. 16)

$$\text{P- bending} = \frac{(M_{left} - M_{right})}{L_h} \times 2 \times \cos(\theta) \quad (6)$$

$$L_h = L_{Beam} - 2 \times S_h \quad , \quad S_h = t_p + L_{stiffner} \quad (7)$$

As shown in Fig. 18, specimens have approximately up to 4% rotational capacity without the catenary action, while this value is tripled and is about 12% with its presence. In these diagrams, as the amount of bending force increases, the catenary action load decreases, and they have a vice versa relationship with each other. As a result, the contribution of catenary action should be considered in the acceptance criteria of rotation capacities.

5. Implementing the theoretical model for prediction of the connection's capacity

In this section, according to the results obtained from numerical analyzes, a formula is presented to estimate the maximum capacity of systems with eight bolt stiffened end plate connections. Fig. 16 shows the free diagram assumed in the column removal analysis and the force equilibrium in the middle column. According to this figure, in a column removal scenario, two important forces in determining the amount of these connections capacity are the amount of plastic moment on the column face and the catenary action load in the beam.

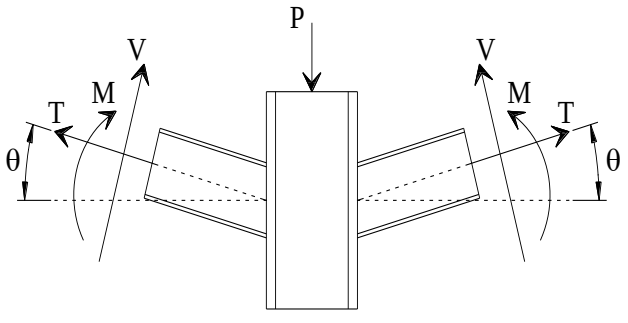

Fig. 16 The free body diagram showing force and moment in column removal analysis

Based on Fig. 16, the system's maximum capacity in a column removal scenario can be written as Eq. 8:

$$P_T = V' + T' \quad (8)$$

V' is the axial force based on the force equation in the plastic hinge, and T' is the corresponding force due to catenary action. The equal force with plastic hinge moment can be defined as Eq. 9:

$$V' = \left(\frac{4 \times \lambda \times M_P}{L_h}\right) \times \cos(\theta) \quad (9)$$

Where M_P is the plastic moment, λ is a coefficient to consider the plastic interaction between bending moment (M) and axial force (N) at a plastic beam region which can be expressed by the Eq. 10, L_h is the distance between plastic hinge locations, and θ is the beam rotation (rad) at the maximum capacity point of the specimen and can be written as Eq. 11:

$$\left(\frac{M}{M_P}\right)^2 + \left(\frac{N}{N_P}\right)^2 = 1 \quad (10)$$

$$\theta = \text{Arc}\tan\frac{\Delta}{L_h} \quad (11)$$

M and N are the moments and axial force, Mp is the plastic bending capacity, and Np is the critical section's axial capacity and Δ is the vertical displacement at the maximum capacity point of the specimen. The corresponding force with catenary action can be computed by Eq. 12:

$$T' = 2 \times T \times \sin(\theta) \quad (12)$$

T is the tensile resistance of connection and obtains from Eq. 13. In this equation, β is the ratio of the stress in the cross-section to the yield stress and is considered as 0.33 based on the numerical analysis. Also, A is the beam cross-section, and F_y is the yield stress.

$$T = \beta \times F_y \times A \quad (13)$$

Up to this point, only one parameter, the vertical displacement at the maximum capacity point ($\Delta_{predict\text{-}max}$), is unknown. The Least Square Method was used for predicting this parameter. When the number of equations is more than the number of unknowns in sets of equations, the LSM is a standard procedure in regression analysis to estimate this overdetermined systems' solution. This method is popular among researchers [42], and generally, the predictive model developed based on the LSM is simple; however, its accuracy should be investigated to be used as a reliable model. Hence, in this study, according to values in Table 5, the LSM was utilized to propose an alternative nonlinear model (see Eq. 14) to predict the vertical displacement at the maximum capacity point ($\Delta_{predict\text{-}max}$).

Table 5
The predicted values of ΔFE-max and the performance of the proposed LSM-based model

Model No.	d_{beam} (mm)	Z_x (mm^3)	$\Delta_{FE\text{-}max}$ (mm)	$\Delta_{predict\text{-}max}$ (mm)	Absolute Error (%)
Specimen 1	533.40	2359737.22	618.72	613.23	0.9
Specimen 2	538.48	2818575.01	573.05	592.16	3.23
Specimen 3	548.64	3621541.14	636.44	625.87	1.69
Specimen 4	607.06	3277412.80	659.83	640	3.1
Specimen 5	617.22	4162314.26	611.77	611.17	0.1
Specimen 6	622.30	4588377.92	614.37	626.55	1.94
Specimen 7	756.92	5669924.14	721.70	747.68	3.47
Specimen 8	762.00	6194310.19	726.48	728.53	0.28
Specimen 9	767.08	6685922.11	739.11	714.79	3.4

* The average absolute percentage error (AAE): 2.01%

* The maximum absolute percentage error (MAE): 3.47%

$$\Delta_{predict-max} = 1.745 \times A^{6.253} \times d^{7.124} \times b_f^{-1.226} \times Z_x^{-6.199} \quad (14)$$

The proposed LSM-based model's performance was evaluated using performance measures AAE and MAE, which are the average absolute percentage error (AAE) and the maximum absolute percentage error (MAE). The AAE was calculated using Eq. 15. In this equation, T_i and N are the predicted output, the actual output obtained from the numerical analysis, and the number of samples. For the proposed predictive model, AAE and MAE values are 2.01% and 3.47%, indicating the proposed model's accuracy.

$$AAE = \frac{1}{N}\sum_{i=1}^{N}\left[\frac{|Y_i - T_i|}{T_i} \times 100\right] \quad (15)$$

Based on the formula presented for displacement at a maximum capacity of eight bolt stiffened extended endplate moment connections, the theoretical values (P_T) of $P_{FE\text{-}max}$ are obtained and presented in Table 6. The values of AAE and MAE are 5.34% and 8.15%, indicating the proposed model's high accuracy level.

Table 6
The predicted values of PFE-max

Model No.	L_h (mm)	A (mm^2)	$P_{FE\text{-}max}$ (kN)	Mp (N.mm)	θ (rad)	T (N)	T' (N)	P_T (kN)	Error (%)
Specimen 1	5561.05	11806.43	1025.32	978288056.32	0.11	1404551.71	309138.85	969.36	5.46%
Specimen 2	5615.66	13870.94	1154.41	1168510733.94	0.11	1650156.38	347368.86	1128.70	2.23%
Specimen 3	5743.93	17612.87	1497.59	1501400419.77	0.11	2095314.84	455713.60	1436.85	4.06%
Specimen 4	6451.32	14451.58	1188.48	1358733411.56	0.10	1719232.69	340553.87	1131.90	4.76%
Specimen 5	6566.89	17870.93	1470.46	1725591432.68	0.09	2126015.43	395160.93	1383.07	5.94%
Specimen 6	6627.85	19548.35	1600.18	1902226776.18	0.09	2325569.22	439032.44	1517.90	5.14%
Specimen 7	8243.29	20451.57	1599.93	2350608802.00	0.09	2433021.26	440751.46	1513.05	5.43%
Specimen 8	8297.90	22064.47	1744.25	2568006147.85	0.09	2624899.91	460325.30	1624.38	6.87%
Specimen 9	8358.86	23548.34	1879.32	2771816159.58	0.09	2801428.27	478532.88	1726.06	8.15%

* The average absolute percentage error (AAE): 5.34%

* The maximum absolute percentage error (MAE): 8.15%

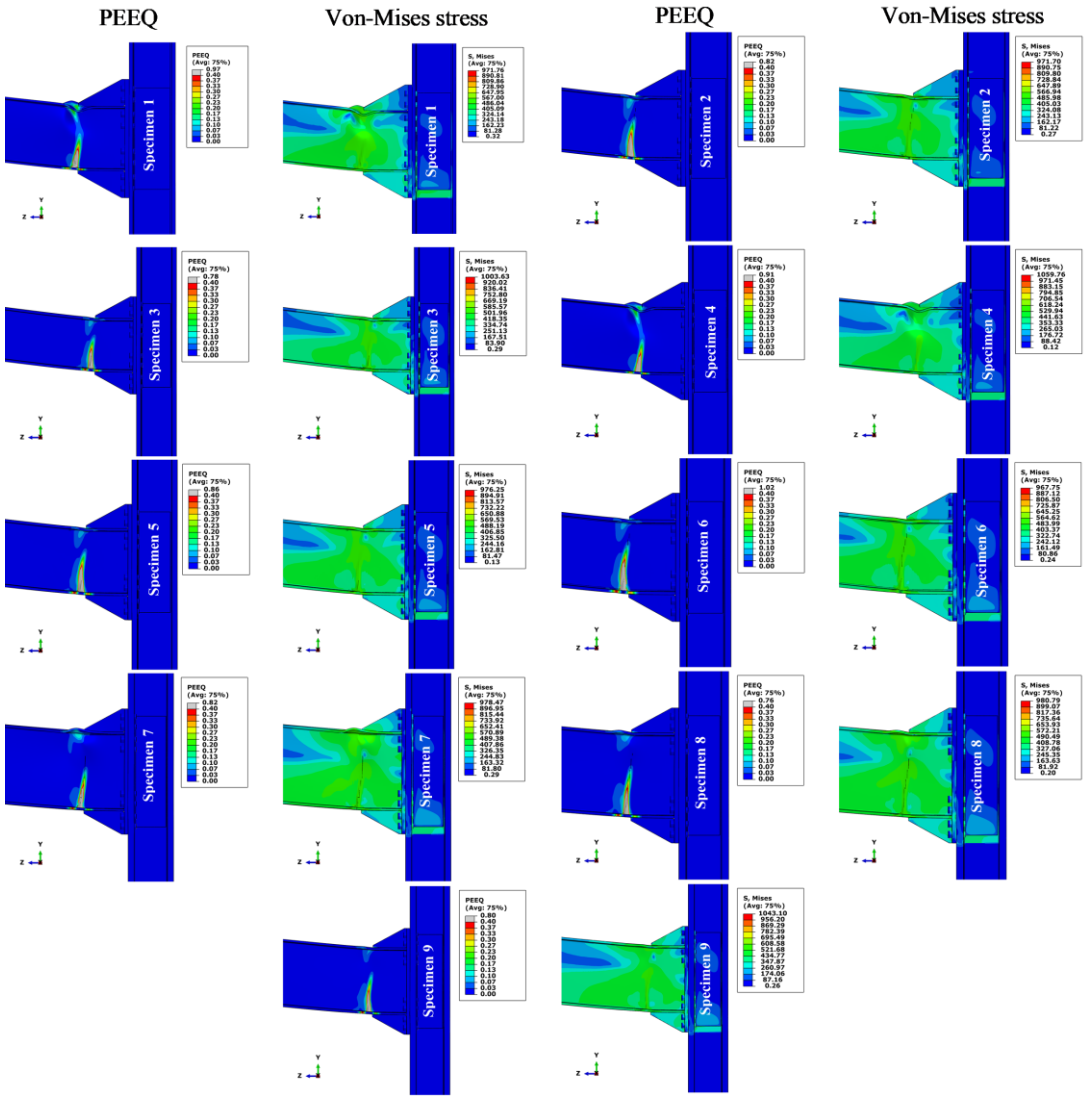

Fig. 17 The deformation, PEEQ, and Von-Mises stress contour for nine specimens

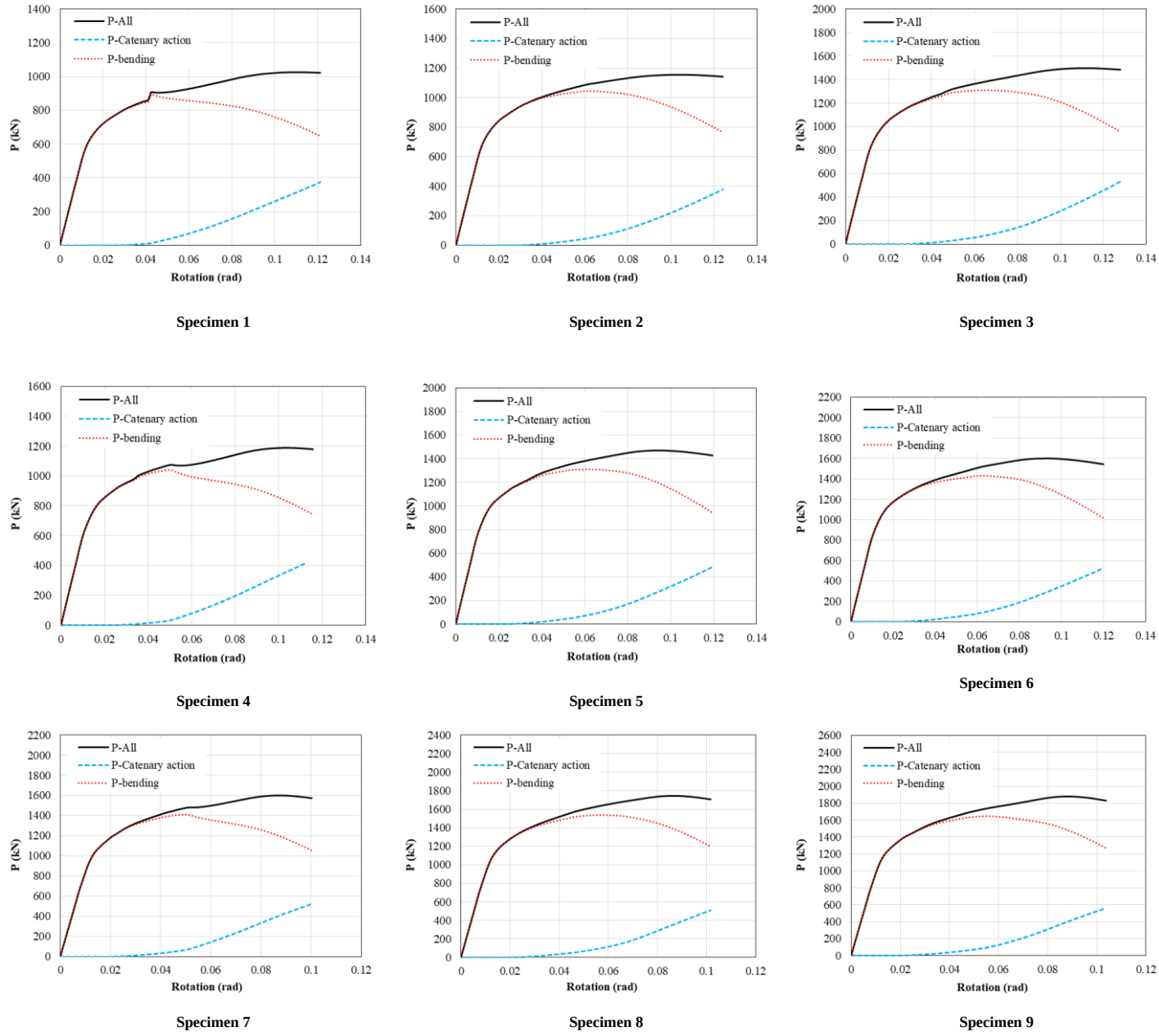

Fig. 18 Summary of Force-rotation angle of nine numerical specimen

6. Conclusion

In this study, the behavior of eight bolt extended endplate moment connections and their maximum capacity subjected to the column removal scenario has been investigated. In this regard, a verification of composite of three columns and two beams under column removal scenario using finite element modeling against valuable experimental results presented by Dinu et al. [24] has done, and fracture modes of the analytical model have been discussed. Based on the verification model, nine 8ES endplate moment connections were designed by the [27, 37, 38]. The significant results of this research based on the FE results can be drawn:

1. Based on these nine specimens' failure mode, the beam properties significantly affect these connections' maximum capacity.

2. The effect of four parameters of d_{beam}, Z_x, b_f/t_f, and d_{bolt} has been investigated on specimens' maximum capacity. It can be observed that based on the regression method results, parameters like the cross-section of the beam (A), beam depth (d_{beam}), flange width (b_f), plastic section modulus (Z_x), and bolt diameter (d_{bolt}) have a correlation coefficient of more than 80% unlike the parameter b_f/t_f (R=28%) with a maximum capacity of specimens.

3. Regarding the Least Square Method, a formula derived to determine the displacement at the maximum force capacity of connections. The performance measures of AAE and MAE for this formula were 2.01% and 3.47%, respectively.

4. According to the proposed theoretical model in section 5, a procedure has been conducted to determine the maximum capacity of 8ES connections. The performance measures of AAE and MAE for the proposed method were 5.34% and 8.15%.

References

[1] Administration, T. U. S. G. S., "Progressive collapse analysis and design guidelines for new federal office buildings and major modernization projects", Journal, GSA, Issue, 2003.
[2] (UFC), U. f. c., "Design of building to resist progressive collapse", 2016.
[3] Daneshvar, H., "One-sided steel shear connections in column removal scenario", 2013.
[4] Brett, C. and Lu, Y., "Assessment of robustness of structures: Current state of research", Frontiers of Structural and Civil Engineering, 7, 4, 356-368, 2013.
[5] Astaneh-Asl, A., et al., "Progressive collapse resistance of steel building floors", Report Number UCB/CEE-Steel-2001, 3, 2001.
[6] Khandelwal, K. and El-Tawil, S., "Collapse behavior of steel special moment resisting frame connections", Journal of Structural Engineering, 133, 5, 646-655, 2007.
[7] Sadek, F., et al., "An experimental and computational study of steel moment connections under a column removal scenario", NIST Technical Note, 1669, 2010.
[8] Demonceau, J.-F., "Steel and composite building frames: sway response under conventional loading and developmet of membrane effects in beams further to an exceptional action", Université de Liège, 2008.
[9] Karns, J. E., et al., "Behavior of varied steel frame connection types subjected to air blast, debris impact, and/or post-blast progressive collapse load conditions", Structures Congress 2009: Don't Mess with Structural Engineers: Expanding Our Role. 2009.
[10] Yang, B. and Tan, K., "Behaviour of steel beam-column joints subjected to catenary action under a column-removal scenario", Journal of Structural Engineering, ASCE. Submitted for

publication, 2010.
[11] Yang, B. and Tan, K. H., "Numerical analyses of steel beam–column joints subjected to catenary action", Journal of Constructional Steel Research, 70, 1-11, 2012.
[12] Yang, B. and Tan, K. H., "Robustness of bolted-angle connections against progressive collapse: Experimental tests of beam-column joints and development of component-based models", Journal of Structural Engineering, 139, 9, 1498-1514, 2013.
[13] Yang, B. and Tan, K. H., "Experimental tests of different types of bolted steel beam–column joints under a central-column-removal scenario", Engineering Structures, 54, 112-130, 2013.
[14] Meng, B., Zhong, W., and Hao, J., "Anti-collapse performances of steel beam-to-column assemblies with different span ratios", Journal of Constructional Steel Research, 140, 125-138, 2018.
[15] Barmaki, S., Sheidaii, M. R., and Azizpour, O., "Progressive Collapse Resistance of Bolted Extended End-Plate Moment Connections", International Journal of Steel Structures, 1-15, 2020.
[16] Lew, H. S., et al., "Performance of steel moment connections under a column removal scenario. I: Experiments", Journal of Structural Engineering, 139, 1, 98-107, 2013.
[17] Li, L., et al., "Experimental investigation of beam-to-tubular column moment connections under column removal scenario", Journal of Constructional Steel Research, 88, 244-255, 2013.
[18] Li, L., et al., "Effect of beam web bolt arrangement on catenary behaviour of moment connections", Journal of Constructional Steel Research, 104, 22-36, 2015.
[19] Qin, X., et al., "Experimental study of through diaphragm connection types under a column removal scenario", Journal of Constructional Steel Research, 112, 293-304, 2015.
[20] Qin, X., et al., "A special reinforcing technique to improve resistance of beam-to-tubular column connections for progressive collapse prevention", Engineering Structures, 117, 26-39, 2016.
[21] Yan, S., et al., "Experimental evaluation of the full-range behaviour of steel beam-to-column connections", Advanced Steel Construction, 16, 1, 77-84, 2020.
[22] Faridmehr, I., et al., "An overview of the connection classification index", Advanced Steel Construction, 15, 2, 145-156, 2019.
[23] Arul Jayachandran, S., et al., "Investigations on the behaviour of semi-rigid endplate connections", Advanced Steel Construction, 5, 4, 432-451, 2009.
[24] Dinu, F., Marginean, I., and Dubina, D., "Experimental testing and numerical modelling of steel moment-frame connections under column loss", Engineering Structures, 151, 861-878, 2017.
[25] "Abaqus 6.14 Analysis User's Manual", Journal, Dassault Systems, Issue, 2014.
[26] Krolo, P., Grandić, D., and Bulić, M., "The guidelines for modelling the preloading bolts in the structural connection using finite element methods", Journal of Computational Engineering, 2016, 2016.
[27] ANSI, B., "AISC 360-16, Specification for Structural Steel Buildings", Chicago AISC, 2016.
[28] Seif, M., et al., "Finite element modeling of structural steel component failure at elevated temperatures", Structures. 2016. Elsevier.
[29] Dolbow, J. E., "An extended finite element method with discontinuous enrichment for applied mechanics", 2000.
[30] Abou-zidan, A. and Liu, Y., "Numerical study of unstiffened extended shear tab connections", Journal of Constructional Steel Research, 107, 70-80, 2015.
[31] Suleiman, M. F., "Non-Linear Finite Element Analysis of Extended Shear Tab Connections", Cincinnati, Ohio, USA, 2013.
[32] Morrison, M., Quayyum, S., and Hassan, T., "Performance enhancement of eight bolt extended endplate moment connections under simulated seismic loading", Engineering Structures, 151, 444-458, 2017.
[33] Naimi, S., Celikag, M., and Hedayat, A. A., "Ductility enhancement of post-Northridge connections by multilongitudinal voids in the beam web", The Scientific World Journal, 2013, 2013.
[34] Raftari, M., Mahjoub, R., and Hekmati, A., "Evaluation of Damage Indicators of Weld and Cyclic Response of Steel Moment Frame Connection Using Side Stiffener Plates", AUT Journal of Civil Engineering, 1, 1, 67-76, 2017.
[35] Rahnavard, R., Hassanipour, A., and Siahpolo, N., "Analytical study on new types of reduced beam section moment connections affecting cyclic behavior", Case Studies in Structural Engineering, 3, 33-51, 2015.
[36] Ricles, J. M., et al., "Development of improved welded moment connections for earthquake-resistant design", Journal of Constructional Steel Research, 58, 5-8, 565-604, 2002.
[37] Seismic, A., "Seismic Provisions for Structural Steel Buildings,(ANSI/AISC 341-16)", Journal, American Institute of Steel Construction, Chicago, IL, Issue, 2016.
[38] AISC, A., "AISC 358-16", Prequalified connections for special and intermediate steel moment frames for seismic applications. Chicago (IL): American Institute of Steel Construction, 2016.
[39] Ahmadi, R., et al., "Experimental and numerical evaluation of progressive collapse behavior in scaled RC beam-column subassemblage", Shock and Vibration, 2016, 2016.
[40] Sadek, F., et al., "Performance of steel moment connections under a column removal scenario. II: Analysis", Journal of Structural Engineering, 139, 1, 108-119, 2013.
[41] Zhong, W., Meng, B., and Hao, J., "Performance of different stiffness connections against progressive collapse", Journal of Constructional Steel Research, 135, 162-175, 2017.
[42] Marquardt, D. W., "An algorithm for least-squares estimation of nonlinear parameters", Journal of the society for Industrial and Applied Mathematics, 11, 2, 431-441, 1963.